

# Separation of multiple echoes using a high-resolution spectral analysis for SuperDARN HF radars

Laurent Barthès, R. André, J.-C Cerisier, J.-P Villain

▶ **To cite this version:**

Laurent Barthès, R. André, J.-C Cerisier, J.-P Villain. Separation of multiple echoes using a high-resolution spectral analysis for SuperDARN HF radars. Radio Science, 1998, 33 (4), pp.1005-1017. 10.1029/98RS00714 . insu-02183268

**HAL Id: insu-02183268**

**https://insu.hal.science/insu-02183268**

Submitted on 15 Jul 2019

**HAL** is a multi-disciplinary open access archive for the deposit and dissemination of scientific research documents, whether they are published or not. The documents may come from teaching and research institutions in France or abroad, or from public or private research centers.

L'archive ouverte pluridisciplinaire **HAL**, est destinée au dépôt et à la diffusion de documents scientifiques de niveau recherche, publiés ou non, émanant des établissements d'enseignement et de recherche français ou étrangers, des laboratoires publics ou privés.

*Radio Science*, Volume 33, Number 4, Pages 1005–1017, July–August 1998

# Separation of multiple echoes using a high-resolution spectral analysis for SuperDARN HF radars

L. Barthes,[1] R. André,[2] J.-C. Cerisier,[1,3] and J.-P. Villain

**Abstract.** Data obtained with coherent HF backscatter radars of the Super Dual Auroral Radar Network (SuperDARN) are routinely analyzed with a standard algorithm based upon the simplifying assumption that the backscattered signal consists of a single source, characterized by its Doppler velocity and spectral width. More complex situations are often encountered where the signal includes several sources, either due to the additional existence of ground scatter or due to multiple ionospheric lines, related to a strongly inhomogeneous velocity field. We analyze the response of the standard algorithm to such signals and we propose to use high-resolution spectral analysis methods, namely, the multiple signal classification (MUSIC) method, to separate multiple echoes with different velocity and spectral width. We analyze theoretically the autocorrelation function of the received signal, and we show that its structure satisfies the criteria for processing by the MUSIC algorithm. A statistical numerical simulation of SuperDARN data processing by the MUSIC method allows us to evaluate the performances and the limits of applicability of the method. We show and illustrate with examples taken from experimental data that the main improvements are (1) the correct separation of mixed echoes from ground and ionosphere, which enhances the quality of ionospheric convection measurements, and (2) the capability to resolve multiple ionospheric sources which appear in regions of inhomogeneous convection. These multiple sources can be used to resolve small-scale structures in the velocity field.

## 1. Introduction

The Super Dual Auroral Radar Network (SuperDARN) coherent HF radars have been designed to monitor the large-scale ionospheric convection [*Greenwald et al.*, 1995]. From the signal coherently backscattered by electron density irregularities frozen in the ionospheric plasma, the radial component of the convection velocity can be deduced. Using two radars situated at remote sites and sharing a common field of view, a vector convection map can be obtained. The transmitted signal consists in a multipulse sequence, a technique initially developed by *Farley* [1972] for incoherent radars and successfully applied to HF radars by *Greenwald et al.* [1985]. The Doppler velocity is derived from the complex autocorrelation function (ACF) of the signal returned from the ionosphere. The ACF generally fits a damped complex sine wave. The slope of the time variation of the phase gives the Doppler velocity, and the spectral width is related to the damping factor. Occasionally, the ACF is more complex, as can be expected when several sources are simultaneously present in the target. The most common case is that of an ionospheric source superimposed to a ground echo. Some cases also result from two simultaneous ionospheric echoes produced by a velocity shear present in a single radar cell. When interpreted as a single damped sine wave, these complex ACFs lead usually to erroneous values of the velocity and spectral width. In this study, we focus our attention on these cases in order to separate the contribution of the different sources to the ACF. Because of the small number of points of the ACF (typically 17-20), the

[1]Centre d'Etude des Environnements Terrestre et Planétaires, UVSQ/CNRS, Saint-Maur-des-Fossés, France
[2]Laboratoire de Physique et Chimie de l'Environnement, CNRS, Orléans, France
[3]Also at Université Pierre et Marie Curie, Paris, France.

Copyright 1998 by the American Geophysical Union.

Paper number 98RS00714.
0048-6604/98/98RS-00714$11.00

frequency resolution of the Fourier transform method is not sufficient. A high-resolution method is more appropriate, namely, the multiple signal classification (MUSIC) method described by *Schmidt* [1986].

The standard processing technique of the radar data, which is valid in the case of a single source, will be briefly reviewed in section 2. In section 3, we will consider the case of two sources. The structure of the ACF is investigated theoretically, and examples taken from the SuperDARN radars will illustrate the inadequacy of the standard method in that case. The alternate method based on the MUSIC algorithm will be described in section 4, and a statistical evaluation of its capability to provide correct results will be presented. Finally, section 5 will discuss examples illustrating the potential benefits of the high-resolution spectral analysis for geophysical purposes.

## 2. The Standard Analysis

Before investigating the case of several sources, let us recall the standard situation when a single source is present and investigate how the standard method of analysis works. We will first describe the multipulse emission scheme and its processing to calculate the ACF. We will then present how the physical parameters, velocity, and spectral width are extracted by the standard method.

### 2.1. Multipulse and Autocorrelation Function

The main advantages of a multipulse system have been thoroughly described by *Farley* [1972]. The basic principle is to transmit a sequence of pulses such that the time delays between any two pulses of the sequence are different and form a regular series, thus allowing us to calculate the corresponding delays of the ACF. The pulse length defines the range resolution or, equivalently, the radial length of the elementary cell in the radar field of view. One of the multipulse schemes currently used by the SuperDARN radars is shown in Figure 1. The basic scheme has evolved slightly with time, but the main characteristics remain similar to those used in this study. The pulse length is 300 μs, giving a resolution of 45 km in range. The time separation between pulses is an integer multiple of $\tau_0 = 2.4$ ms. When receiving, the radar signal is digitized with a sampling period of 300 μs, equal to the pulse length. From the seven-pulse sequence, 17 delays of the ACF are calculated. The total signal received at a given time is the sum of the signals backscattered from

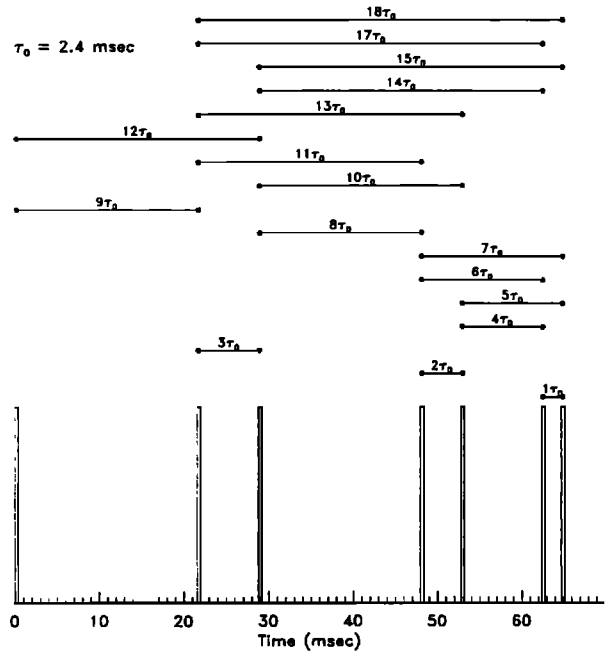



**Figure 1.** Example of a seven-lag multipulse scheme used by the Super Dual Auroral Radar Network (SuperDARN) radars. This sequence allows determining 17 points of the autocorrelation (ACF) function of the backscattered signal.

different ranges and corresponding to the pulses previously transmitted. For instance, 33 ms after the start of the pulse sequence, the received signal will be the sum of the echoes backscattered at ranges 1710 km (from the second pulse of the sequence) and 630 km (from the third pulse). The echo backscattered from the range 4950 km (first pulse) can be neglected, because echoes returning from ranges over 3500 km are usually too faint. The received signal can be written:

$$S_0 = A_1 e^{-j\omega_1 t_0} + A_2 e^{-j\omega_2 t_0} e^{-j\Phi_2} \qquad (1)$$

where $t_0$ is the time of the measurement, here 33 ms; $\omega_1$ and $\omega_2$ are the angular frequencies of the signals backscattered from ranges 1710 and 630 km, respectively; and $A_1$ and $A_2$ are the associated amplitudes. The phase $\Phi_2$ is the phase difference between the two signals. In order to calculate the ACF for the range 1710 km and for the delay $\tau$ (for instance, $\tau = 3\tau_0$), we use also the signal received at time $t_0 + \tau$ (here 40.2 ms):

$$S_\tau = A_1 e^{-j(\omega_1 t_0 + \tau)} + A_3 e^{-j\omega_3 (t_0 + \tau)} e^{-j\Phi_3} \qquad (2)$$

This signal is also the sum of two echoes, one from the range 1710 km with the amplitude $A'_1$ (which can be different from $A_1$ because of the time variation of the scattering fluctuations), and one from the unwanted range 2790 km (index 3). The product $S_0 S_\tau^*$ is then

$$\begin{aligned} S_0 S_\tau^* = {} & A_1 A_1'^* e^{j\omega_1 \tau} + \\ & A_2 A_1'^* e^{j(\omega_1-\omega_2)t_0} e^{j\omega_1 \tau} e^{j\Phi_2} + \\ & A_1 A_3^* e^{j(\omega_3-\omega_1)t_0} e^{j\omega_3 \tau} e^{j\Phi_3} + \\ & A_2 A_3^* e^{j(\omega_3-\omega_2)t_0} e^{j\omega_3 \tau} e^{j(\Phi_3-\Phi_2)} \end{aligned} \quad (3)$$

This relation is valid for a single multipulse sequence. Only the first term in the right-hand side of (3) represents the ACF for the range 1710 km and the delay $3\tau_0$. The three remaining terms are cross products between different ranges. Their relative amplitude is reduced by repeating the multipulse scheme. The phases $\Phi_i$ are random variables, due to the incoherence of the phase of the fluctuations which are responsible for the backscatter, at times separated by the delay between successive multipulse sequences, typically 100 ms. The damping of these terms is proportional to $N^{1/2}$, where $N$ is the number of multipulse sequences. A relative damping of 8.6 is obtained when the ACF is averaged over 75 multipulses. From here on, only the first term in (3) will be considered

$$C(\tau) = \left\langle S_0 S_\tau^* \right\rangle = \left\langle A_1 A_1'^* \right\rangle e^{j\omega_1 \tau} \quad (4)$$

This technique allows us to obtain 17 points of the complex ACF in each of the 70 range gates, every 7 s.

### 2.2. Obtaining Velocity and Spectral Width From the ACF

The standard method for obtaining the Doppler velocity and the spectral width has been described by *Villain et al.* [1987]. The velocity is derived from the Doppler frequency, deduced from the phase of the ACF by a linear least squares fit. The phase $\phi$ is given by $\phi = \arctan(I/R)$, where $R$ and $I$ are the real and imaginary parts of the ACF. A typical example taken from the Stokkseyri SuperDARN radar is given in Figure 2a. Dots represent the experimental values of the phase, and the solid line is the least squares fit to these points. In this example, the cross terms in (3) have no influence on the experimental ACF, as expected, thanks to the averaging process. The relation between the Doppler frequency $\omega$ and the velocity $v$ is

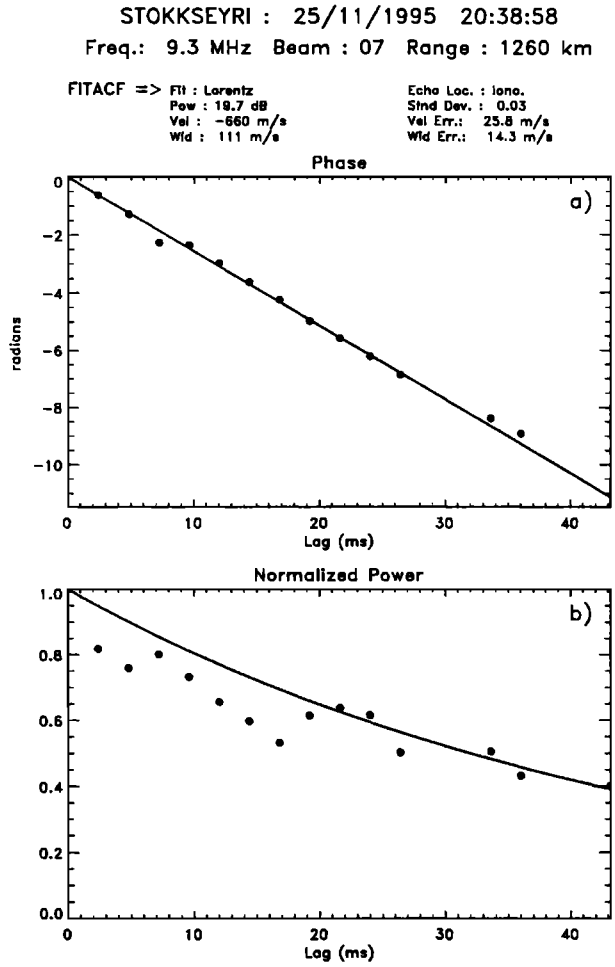



**Figure 2.** Illustration of the "standard" analysis of the SuperDARN ACFs. (a) The Doppler frequency is determined by a linear least squares fit of the phase of the ACF. (b) The spectral width is deduced from the fit of the power to a Gaussian or a Lorentzian spectrum.

$$v = \frac{c}{2\omega_e}\omega \quad (5)$$

where $c$ is the velocity of light and $\omega_e$ is the transmitter frequency. In the above example, the Doppler velocity is -660 m/s. The estimated velocity error remains small, less than 30 m/s.

The spectral width is deduced from the time variation of the power $P(\tau)$ of the ACF $[P = (R^2 + I^2)^{1/2}]$. Two types of fits are performed, one by an exponential profile (Lorentzian spectrum) and one by a Gaussian profile (Gaussian spectrum). These are least squares fits performed on the logarithm of the modulus of the ACF.

The better of the two fits in the least squares sense gives the selected spectral width. The physical meaning of these two models for the shape of the spectrum is discussed below. Figure 2b shows an example of a Lorentzian fit. The relation between the damping factor $\alpha$ and the spectral width $w$ of the Lorentzian spectrum is

$$w = \frac{c}{2\omega_e} 2\alpha \tag{6}$$

In the above example, the spectral width is 111 m/s. The estimated error is less than 15 m/s.

Previous statistical studies [*Villain et al.*, 1987] have shown that about 80% of the ACFs are best fitted by a Lorentzian spectrum. The physical interpretation of these different behaviors is related to the ratio of the correlation length to the radar wavelength. The theory shows that Lorentzian spectra occur when this ratio is larger than unity. *Villain et al.* [1996] have shown that the correlation length is typically 1 m, thus confirming the small value of the above ratio and the observed predominance of Lorentzian spectra. *Hanuise et al.* [1993] have introduced a mixed type of damping of the ACF: Gaussian for short delays and Lorentzian for long delays.

## 3. The Case of Two Sources

The case where two sources are simultaneously present at the same range will now be considered. Owing to propagation conditions, this happens when a ground echo, characterized by a very small Doppler velocity and a narrow spectral width, is present together with an ionospheric echo. From here on, only the averaged form of the ACF, as given by (4), will be considered. Neglecting the damping of the signal, the ACF in the case of two sources can be written

$$C(\tau) = (A_1^2 + \beta)e^{j\omega_1\tau} + (A_2^2 + \beta^*)e^{j\omega_2\tau} \tag{7}$$

with

$$\beta = A_1 A_2 e^{j(\omega_1 - \omega_2)t_0} e^{-j\Phi} \tag{8}$$

Here $\omega_1$ and $\omega_2$ are the frequencies of the two sources; $A_1$ and $A_2$ are their respective real amplitudes; and $\Phi$ is their phase difference. Relation (7) shows that the ACF is now given by the sum of the ACFs of each source, with an additional coupling term. Again, and for the same reasons as for the coupling term between different ranges which appeared in equation (3), this term vanishes with the averaging procedure.

Up to now, the damping of the ACF has been neglected. It can be reintroduced through a velocity (frequency) spread around $\omega$. This spread will cause a damping of all the terms of the ACF. For a Lorentzian damping, the ACF can be written

$$C(\tau) = A_1^2 e^{-\alpha_1\tau} e^{j\omega_1\tau} + A_2^2 e^{-\alpha_2\tau} e^{j\omega_2\tau} \tag{9}$$

From this relation, it is clear that the time variation of the phase of the ACF is no longer linear. Figure 3a shows the variation of the phase for the case of two sources, a ground echo ($A_1 = 0.7$, $V_1 = 0$, $\alpha_1 = 0$) and an ionospheric source ($A_2 = 1$, $V_2 = 200$ m/s, $\alpha_2 = 150$ m/s). The phase oscillates around zero, and it is clear from the figure that the standard method is not appropriate. It is important to notice that the linear least squares fit of the phase leads to a small value of the velocity (11 m/s in the present example), thus suggesting that the standard method is able to detect the ground echo. However, the determination of the spectral width is completely erroneous (166 m/s instead of 0 m/s). This is extremely important because the usual criteria for identifying ground echoes are based on their physical characteristics, namely, a small velocity associated to a narrow spectral width. The present simulation is typical of a false identification of an ionospheric echo with a small velocity, whereas the ACF represents an ionospheric velocity of 150 m/s superimposed to a ground echo. Let us remark, however, that the above confusion can be detected by a careful analysis of the quality of the fits of the phase and amplitude.

In Figure 3b, representing experimental data, a behavior similar to the simulation of Figure 3a is observed. The linear fit leads to an almost horizontal slope on which an oscillation is superimposed. The small value of the slope is indicative of a small velocity which can be related to a ground echo, while the faster oscillation is indicative of an ionospheric source having a velocity of the same order as in the simulation of Figure 3a. Figure 3c is a second experimental example where now the larger slope of the fit indicates a larger velocity. This large slope, together with the superimposed oscillation, suggests the presence of two ionospheric sources.

## 4. The High-Resolution MUSIC Method

In the case of short data sequences, the Fourier transform technique provides poor spectral resolution. In recent years, new spectral analysis methods have

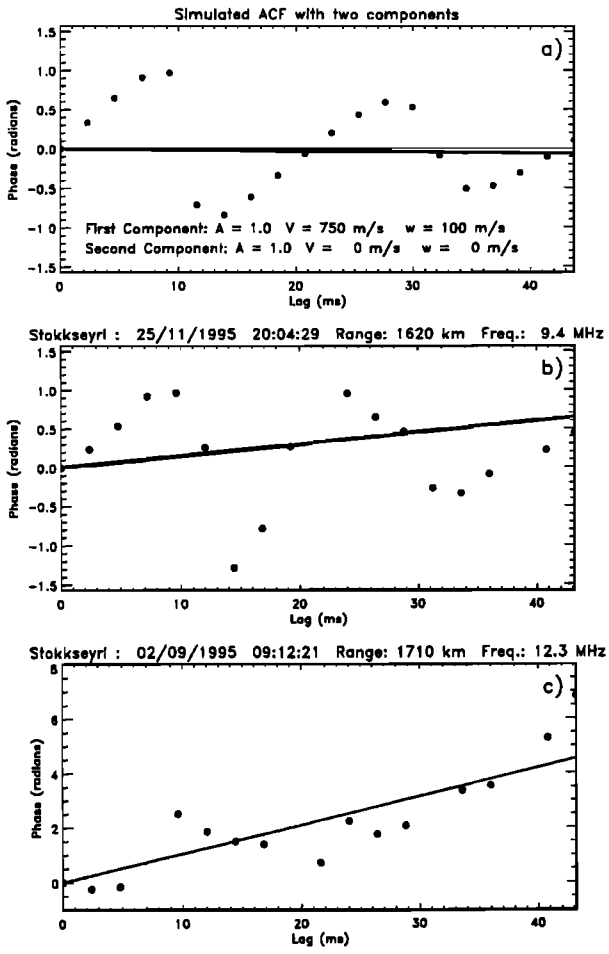



**Figure 3.** Phase (dots) of the ACF when two sources are simultaneously present in the backscattered signal. (a) Simulated ACF with ground and ionospheric echoes. (b) Experimental ACF with ground and ionospheric echoes. (c) Experimental ACF with two ionospheric echoes. The solid line represents the fit of the phase by the standard (single source) method.

appeared which are designed to enhance the spectral resolution. They are all based on a priori hypotheses on the structure of the signal. Among them, the multiple signal classification (MUSIC) method, described by *Schmidt* [1986], assumes a signal composed of a sum of complex sine waves with additional white noise. The structure of the ACF given by (9) suggests that this method is appropriate to the SuperDARN data.

### 4.1. Summary of the MUSIC Method

Let us now write the ACF as a sum of $M$ damped sine waves.

$$C_n = C(n\tau_0) = \sum_{i=1}^{M} A_i z_i^{n\tau_0} \tag{10}$$

with

$$z_i = e^{-\alpha_i + j\omega_i} \tag{11}$$

Let $\mathbf{Y}_n$ be the vector built with $p$ consecutive observations organized in reverse order :

$$\mathbf{Y}_n = [C_n, C_{n-1}, \cdots, C_{n-p+1}]^{\mathrm{T}} \tag{12}$$

The $p \times p$ autocorrelation matrix $\mathbf{R}_p$ is defined as the expectation of $\mathbf{Y}_n \mathbf{Y}_n^{+}$, where the plus sign denotes the transpose of the complex conjugate. In the presence of damping, the matrix cannot be calculated by the usual method using both direct and reverse order in the $C_n$ series that constitute the $\mathbf{Y}_n$ vector. The matrix is simply calculated as

$$\mathbf{R}_p = E\{\mathbf{Y}_n \mathbf{Y}_n^{+}\} = \frac{1}{N-p+1} \sum_{n=p-1}^{N-1} \mathbf{Y}_n \mathbf{Y}_n^{+} \tag{13}$$

where $E\{\ \}$ is the mathematical expectation operator and $N$ is the length of the data record (the number of points in the ACF). It can be shown that if $C_n$ is given by (10) and if $\mathbf{R}_p$ is estimated with the above equation (13), the rank of $\mathbf{R}_p$ is equal to $M$, which means that only $M$ eigenvalues $\lambda_i$, $i \in [1,p]$, are nonzero values. The $M$ eigenvectors $\mathbf{V}_i$ associated with these eigenvalues span the signal subspace. The signal has only projection in this subspace:

$$\mathbf{R}_p = \sum_{i=1}^{M} \lambda_i \mathbf{V}_i \mathbf{V}_i^{+} \tag{14}$$

The other eigenvectors ($\mathbf{V}_{M+1} .. \mathbf{V}_p$) define the noise subspace (only the noise has projection in this subspace). Owing to the properties of the autocorrelation matrix, these two vector subspaces are orthogonal. Let $\mathbf{Z} = [z^0, z^1, ..., z^{p-1}]^{\mathrm{T}}$ be a vector belonging to the signal subspace. The scalar product between this vector and each of the noise vectors is equal to zero. This property is used to derive the polynom of MUSIC:

$$\sum_{i=M+1}^{p} \left| \mathbf{Z}^{+} \mathbf{V}_i \right|^2 = \mathbf{Z}^{+} . \sum_{i=M+1}^{p} \mathbf{V}_i \mathbf{V}_i^{+} . \mathbf{Z} = \mathbf{Z}^{+} . \mathbf{Q} . \mathbf{Z} \tag{15}$$

The roots of this polynom $z_i$ give through relation (11) the frequencies and damping factors of the sources. The

$M$ signals are associated to the $M$ roots which are closest to the unit circle in the $z$ space.

When white noise is present, it can be shown [*Marple*, 1987] that the eigenvalues of the noisy autocorrelation matrix are equal to those of the nonnoisy matrix plus the noise variance. The method remains the same. When $M$ is unknown, the respective dimensions of the signal space and noise space are determined from the analysis of the sequence, in decreasing order, of the eigenvalues: The signal eigenvalues constitute a decreasing series, whereas the noise eigenvalues are all equal and below the smallest signal eigenvalue. A noise power estimation is thus available. From this value and from the noisy autocorrelation matrix it is easy to get the unnoisy autocorrelation matrix and to derive the power or the signal-to-noise ratio (SNR) of each damped sine wave.

### 4.2. Principle of the Simulation

In order to test the capability of the MUSIC method to derive SuperDARN physical parameters, a large number of simulated ACF have been analyzed. The velocity and the spectral width of the solutions have been systematically calculated. The total number of points in the ACFs is 20, among which are three missing values (lags 6, 7, and 14) called "bad lags," which also occur in the real data, due to interruptions of reception during transmission periods or other perturbations. The dimension of the autocorrelation matrix is chosen to be $p = 8$, which represents a good compromise between the maximum number of sources expected in the signal and the number of points in the ACF. The result of the analysis of each ACF has been attributed one of three possible labels: (1) correct determination (if the velocity is within 50 m/s of the nominal value); (2) false determination (if the velocity is not within 50 m/s of the nominal value); and (3) no determination (if the algorithm identifies only noise, no signal solution being determined).

### 4.3. Single Source

An initial test of the MUSIC algorithm has been performed in the simplest case when the signal consists of a single source. The spectral width has been varied from 0 to 800 m/s by steps of 25 m/s. In each case, the velocity has been varied from -800 m/s to +800 m/s, with a step of 100 m/s. A series of 750 samples have been examined for each velocity and spectral width, with a uniform distribution of the signal-to-noise ratio between 3 and 20 dB. Figure 4 shows the results of the

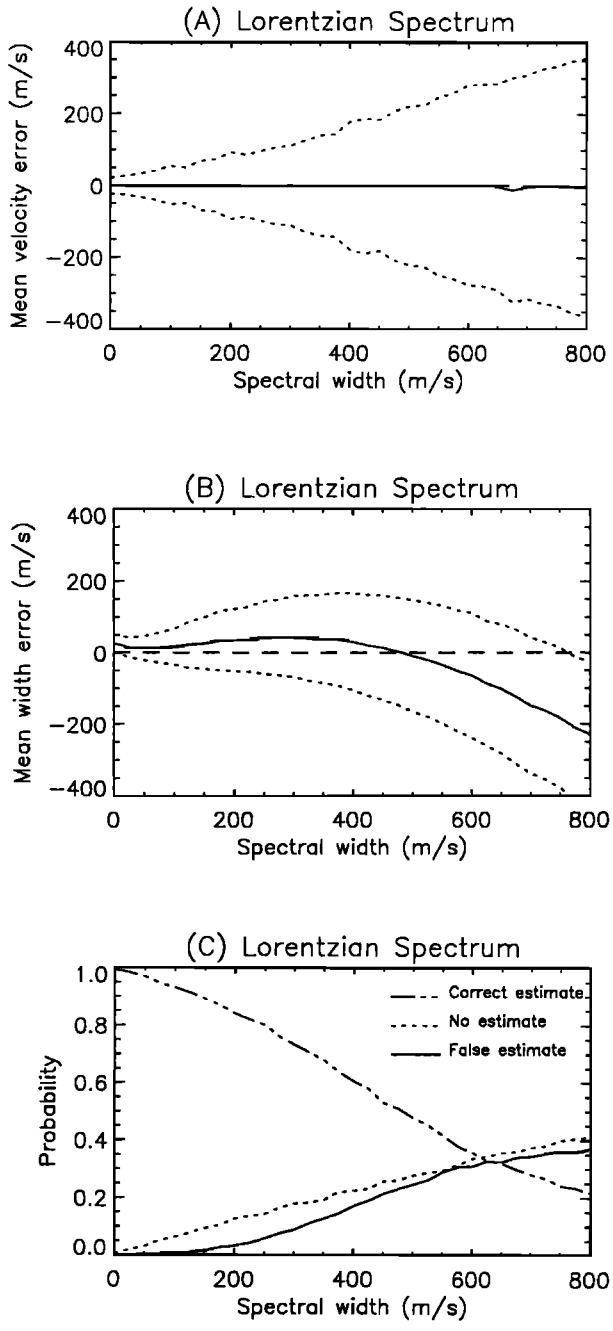



**Figure 4.** Statistical results of the simulation of the analysis of the SuperDARN ACFs with the multiple signal classification (MUSIC) algorithm. (a) Mean error (solid line) and variance (dotted line) in the velocity determination. (b) Mean error (solid line) and variance (dotted line) in the spectral width determination. (c) Probabilities of different results of the MUSIC analysis (correct, false, or no velocity determination). The ACF comprises one single source with a Lorentzian spectrum.

analysis for the case of an exponential decay (Lorentzian spectrum). Figure 4a represents the mean (over velocity and SNR) velocity error as a function of the spectral width. This mean error (solid line) in the velocity determination is zero, which means that the velocity determination remains unbiased, whatever the spectral width. Of course, the standard deviation of the error (dotted lines) increases with spectral width but remains always below the half of the spectral width. It must be observed that when the spectral width is large, the amplitude of the ACF decreases very rapidly and the data for large delays are strongly corrupted by noise, leading to a poor (or impossible) estimate of the parameters of the source. The mean error in the spectral width shown in Figure 4b indicates that the spectral width is slightly overestimated for widths below 500 m/s and underestimated beyond. The bias on the determination of the spectral width can be explained as follows: The roots of the MUSIC polynom associated to the signal are identified by their proximity to the unit circle ($|z_i| = 1$). For large spectral widths, the root moves away from the unit circle and can be confused with roots associated to noise. So only the roots with an underestimated spectral width are close enough to the unit circle to be considered as representing the signal, whereas overestimated values are considered as belonging to the noise subspace and thus rejected.

Figure 4c shows estimates of the probability of a correct estimation of the velocity, the probability of an incorrect determination of the velocity, and the probability that the source is not detected. For small spectral width the probability of a correct detection is very good, whereas the probability of no or false estimation remains negligible. The probability of a false estimation reaches 5% when the spectral width is 250 m/s and 25% when the spectral width is 500 m/s .

The damping of ionospheric backscattered signals is not necessarily exponential. Gaussian damping (leading to a Gaussian spectrum) is sometimes observed, although less often. Although the MUSIC algorithm is not designed for Gaussian damping (two or more close sources can be obtained instead of a single source), the method has been applied to such signals. Figure 5 shows the results of the simulation performed for Gaussian spectra with all other conditions remaining the same as for Figure 4. The main difference is that the probability of a false estimation now reaches only 3% for a spectral width of 250 m/s and raises to 30% for 500 m/s. The probability of no estimation is not different in both cases.

At this point, it is necessary to mention that in the real data, spectral widths larger than 500 m/s are relatively inusual. However, from Figures 4 and 5 it is clear that when such large spectral widths are measured, the results have to be analyzed with great care.

The above simulations have been made with a minimum 3-dB threshold on the estimation of the SNR, whatever the spectral width. Of course, the probability of a false estimation increases with decreasing SNR but also with

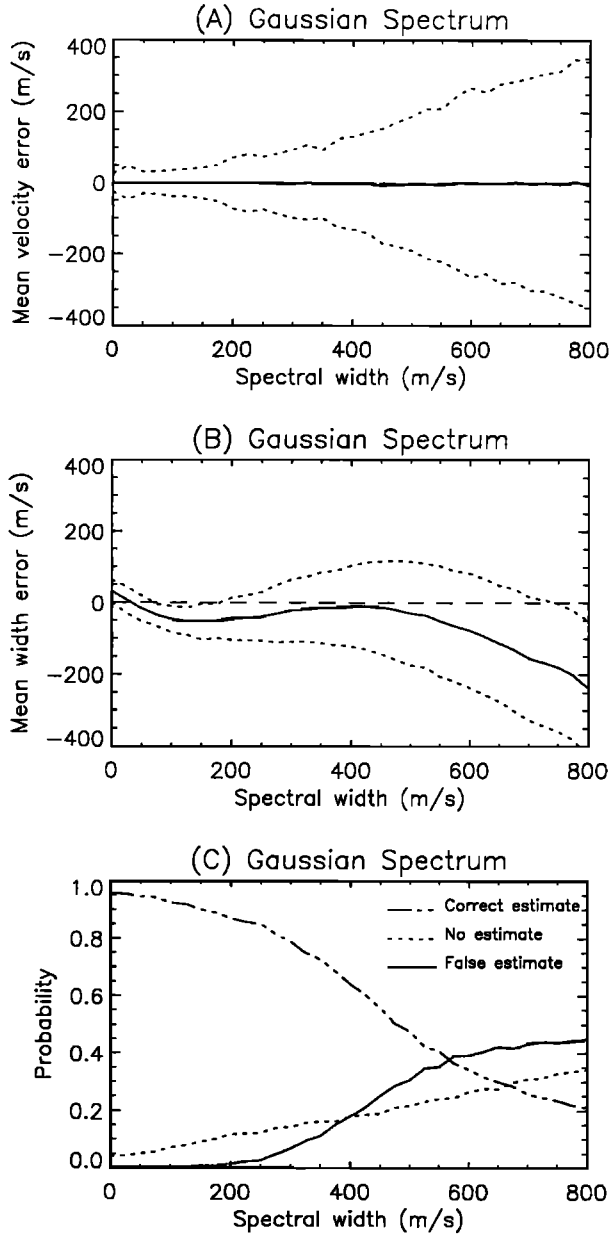



**Figure 5.** Same as Figure 4, but for a Gaussian spectrum.

increasing spectral width. If an upper limit (typically 5%) is set to the probability of a false estimation, a variable SNR threshold has to be used, depending upon the spectral width, a larger value of the threshold being used for larger spectral widths. An analysis of the results of the simulation has led to define an exponential law:

$$SNR_{threshold}(dB) = 4.5 \times \exp(w/450.) \quad (16)$$

which limits the increase in the probability of error to less than 5% for large spectral widths. The above rule, however, is difficult to apply directly because the SNR can be overestimated by MUSIC. This happens when a root of the MUSIC polynom belonging to noise is attributed to a source, thus underestimating the noise level. To avoid this problem, a minimum value of the power for a root of the polynom to be considered as representing a source has been introduced. These two thresholds (minimum SNR and minimum power) have been systematically used in the simulations described below for the case of two sources.

### 4.4. ACF Comprising Two Sources

We now consider the case where two sources are present in the ACF signal. In order to simulate best the most common case of a ground-scattered echo superimposed on an ionospheric echo, one of the simulated signals is characterized by a zero velocity and no damping (zero spectral width). The distribution of the ionospheric sources is similar to the "single source" case presented above with regard to the velocity and spectral width. Both signals have identical amplitudes. Only the case of a Lorentzian spectrum will be discussed here. Two cases must be considered according to whether the velocity difference between the two sources is larger or smaller than the resolution of a Fourier analysis of the ACF (typically 250 m/s). The results are presented in Figure 6, in terms of probabilities, similar to those of Figures 4c and 5c.

When the velocities of the ionospheric and ground echoes have a separation larger than the resolution of a fast Fourier transform (FFT) analysis, the probability of a correct identification of the two sources is the same as for the single source case (Figure 6a). In other words, the estimation of one source does not depend upon the other. This can be demonstrated theoretically from the Cramer Rao boundary [*Delhote*, 1985]. Figure 6a also shows the effect of a SNR threshold. The probability of a false determination is maintained below 5%, whatever the spectral width. The counterpart is a lower

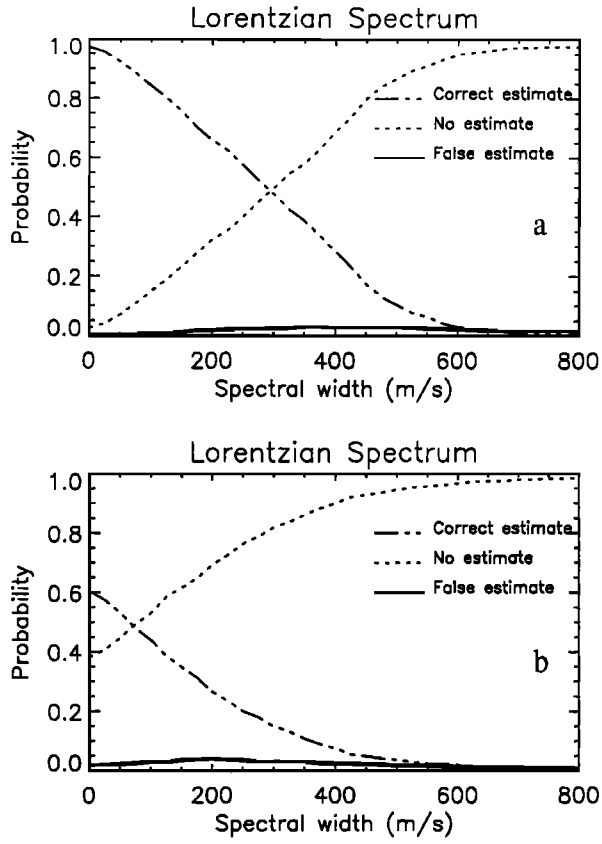



**Figure 6.** Statistical results of the MUSIC analysis when two sources (ionospheric and ground) are present in the signal. The probabilities of different results (correct, false, or no velocity determination) for a Lorentzian ionospheric source are presented. (a) The source separation is larger than the resolution of the Fourier analysis. (b) The source separation is smaller than the resolution of the Fourier analysis.

probability of a correct estimate, typically 50% only for a 300 m/s spectral width. The remaining 45% are rejected by the threshold condition.

Figure 6b shows the results obtained when the ionospheric and ground echoes have velocities too close to be separated by FFT ($\Delta V < 250$ m/s). The probability of a correct estimation is considerably reduced, typically 60% at best. It must be noticed also that the probability of a false estimation, although higher than in the case of two well-separated sources, remains below 5%, whatever the spectral width.

Other simulations have been made for different values of the relative amplitude of the two sources. It can be shown theoretically that the variance of the velocity estimation of an echo does not depend upon the

amplitude of the other [*Delhote*, 1985]. This was confirmed by simulation with ground scatter amplitude up to 30 dB above the ionospheric amplitude.

The simulations have also been analyzed to compare the number of ionospheric sources given by MUSIC to the real number. When only one ionospheric echo is present, the probability of obtaining two or more ionospheric echoes is less than 0.5% in the Lorentzian case, whatever the spectral width, and between 0.5% and 1.5% (depending on the spectral width) in the Gaussian case.

It must be kept in mind that all the above probabilities have been obtained with the ACF of the type defined in section 4.2. Other multipulse schemes can be designed which, by increasing the number of points in the ACF, are potentially able to improve the quality of the results obtained with MUSIC.

## 5. Analysis of SuperDARN Data With the MUSIC Algorithm

SuperDARN data have also been analyzed with the MUSIC algorithm. We present below examples which confirm the capability of high-resolution methods to resolve multiple sources in the scattered signal. We will also illustrate the benefits, which can be obtained by the use of MUSIC for the study of the ionospheric plasma convection.

### 5.1. Ionospheric and Ground Echoes

Figure 7 shows Fourier spectra obtained from the Stokkseyri radar in six adjoining cells (a 3×2 template in range and beam). The data from the two beams are separated by less than 2 min. In the beam-8 panels (left column), the ground echo dominates the FFT spectrum. The standard analysis (not shown in the figure) also detects the ground solution. In addition to the ground echoes, the MUSIC method detects two ionospheric sources: one with a velocity of the order of -350 m/s and one with a positive velocity between 500 and 750 m/s. In the beam-9 panels (right column), the dominant signal is due to the ionospheric negative velocity source. This signal is clearly seen in the FFT spectrum and confirmed by both the MUSIC and standard methods; MUSIC also detects a low velocity solution and the positive velocity ionospheric source. The consistency of the MUSIC determinations in independent cells argues strongly in favor of the method.

Plate 1 shows an example of a SuperDARN radial velocity map. Plate 1a displays the result of the standard analysis. It exhibits both ground echoes (in grey) and ionospheric sources. Plates 1b and 1c display the results of the MUSIC analysis for the same data set. The most intense ionospheric source is shown in Plate 1b and the ground echoes in Plate 1c. The comparison of these three panels shows clearly that MUSIC increases the spatial coverage of ionospheric sources to regions where the standard method could identify only ground echoes. This is particularly the case for the red-orange area which is larger in Plate 1b than in Plate 1a; Comparison also shows that most of the ionospheric echoes identified by the standard method are confirmed by MUSIC. However, some echoes identified as "ionospheric" (green zone in Plate 1a) by the standard method become "ground" by the MUSIC analysis. This means that the spectral width criterion used to distinguish between ground and ionospheric echoes ($w < 50$ m/s) is, in fact, more severe with the standard method than with MUSIC. It must be kept in mind that although the choice of the above limit is based on the analysis of a large number of data, it also contains arbitrariness.

### 5.2. Ionospheric Sources: Comparison With ACF

In order to evaluate the quality of the solution given by a processing algorithm, the ACF can be reconstructed from that solution and compared with the experimental ACF. Figure 8 shows the result of this exercise for both the standard method and MUSIC, in a situation where MUSIC detects two ionospheric sources. Figures 8a and 8b display the real and imaginary parts, respectively. For both components, the MUSIC solution gives a much better fit to the experimental data than the standard analysis. The MUSIC solution in the above example is characterized by two sources with velocities -805 m/s and -253 m/s. The first of these velocities is not far from the value of -711 m/s given by the standard method. This indicates that again, like for the case of a ground echo, the standard analysis can give an estimate of one of the two velocities. However, and again also, the spectral width given by the standard method is strongly overestimated (1036 m/s against 211 m/s). The large spectral width given by the standard method is the consequence of the rapid decay of the ACF, due to the two-component nature of the backscattered signal. It must be noted also that the SNR in this example exceeds 10 dB, a large enough value to rule out an interpretation of the bad

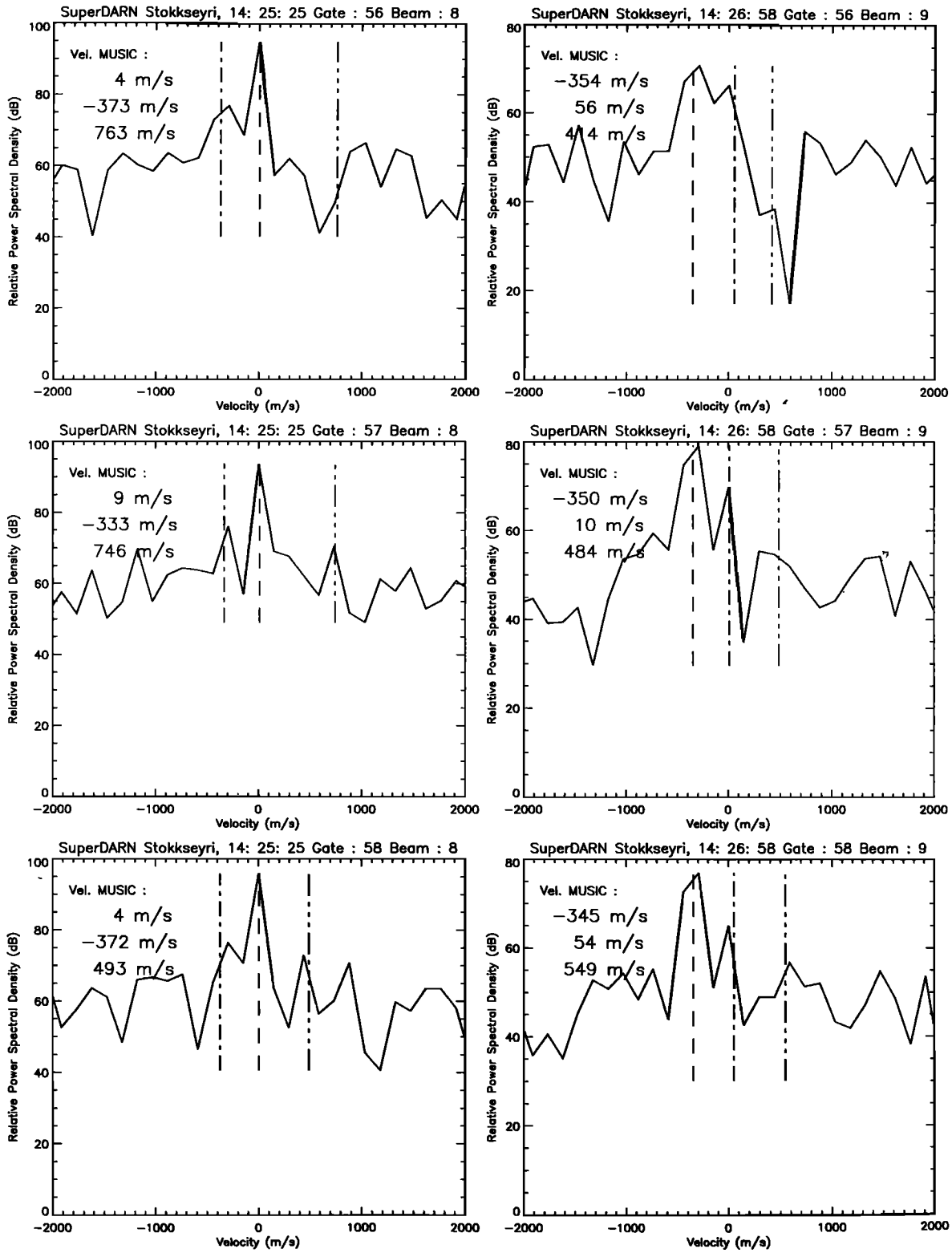



**Figure 7.** Comparison between the results of MUSIC and a fast Fourier transform (FFT) analysis of the ACF in six adjoining cells. The multiple sources detected by MUSIC in the different cells are mutually consistent.

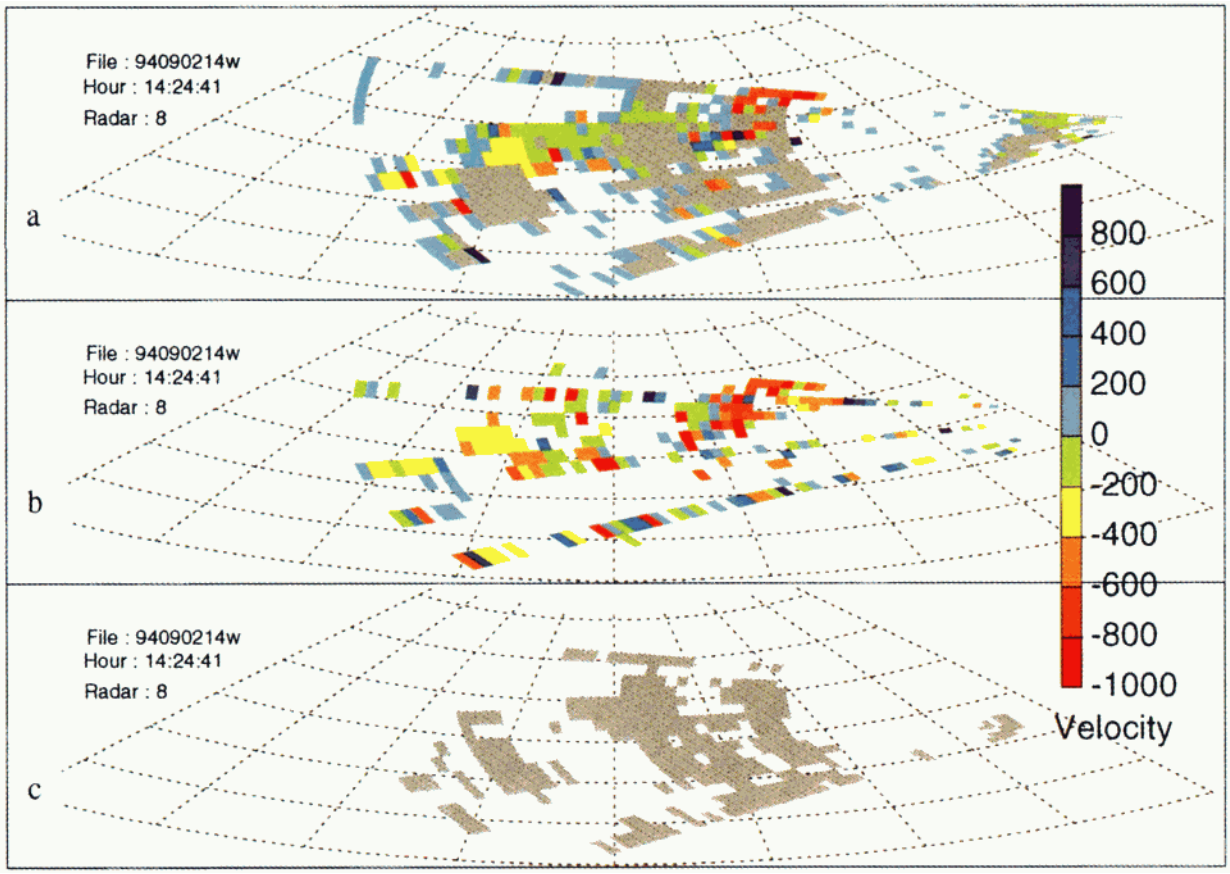



**Plate 1.** Radial velocity maps obtained with the Stokkseyri SuperDARN radar, showing (a) the velocity obtained with the standard analysis; (b) the ionospheric echoes detected by MUSIC; and (c) the ground scatter echoes detected by MUSIC. The coordinates are geographic latitude and longitude.

performance of the standard method in terms of low SNR.

### 5.3. Application to a Convection Velocity Reversal

When a convection velocity reversal is present in the radar field of view, multiple ionospheric sources are expected to be observed in the range gates across which the velocity shear occurs, whereas single sources are expected on both sides of the shear. Figure 9 shows the results obtained with the MUSIC algorithm, for the observation along a fixed direction of a steady shear over a 20-min period. Figure 9a shows the variation of the mean (over the observation period) radial velocity along the radar beam. The position of the shear is clearly identified, with a homogeneous convection on both sides. The probability of multiple sources shown in Figure 9b is close to zero in the two regions of homogeneous flow and shows a significant increase at the location of the velocity shear. The SNR displayed in Figure 9c also shows a maximum at the location of the shear, suggesting that the shear is characterized by an increased level of turbulence responsible for the backscatter of the radar wave. The 10% maximum probability of multiple sources in the shear indicates, however, that multiple ionospheric sources are not a highly common observation, despite favorable conditions.

## 6. Conclusions

We have analyzed the limits of the standard method used for processing SuperDARN HF radar data and based upon the assumption of a single source in the backscattered signal. We have also shown that the

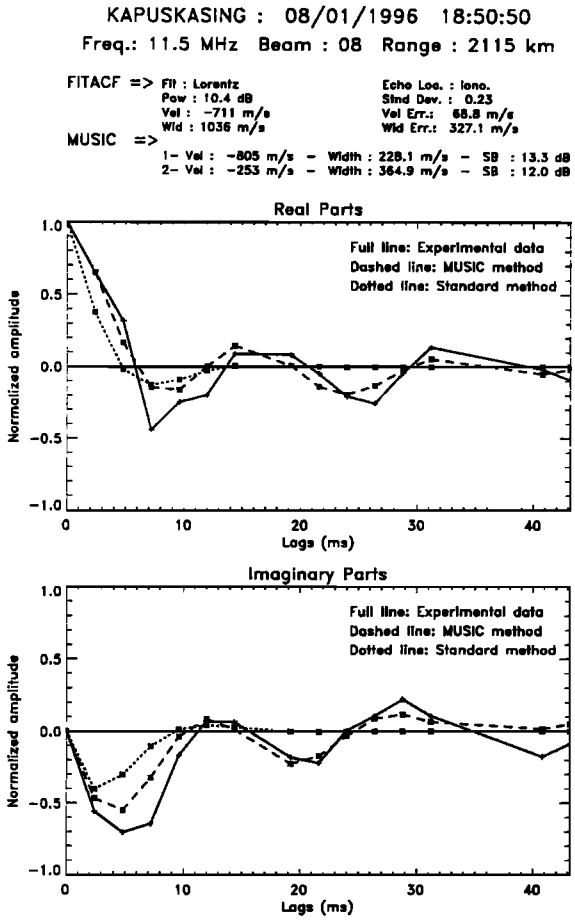



**Figure 8.** Comparison of the results of MUSIC and the standard analysis with the experimental ACF. The MUSIC analysis gives a better fit to the experimental ACF, for both the (top) real and (bottom) imaginary parts.

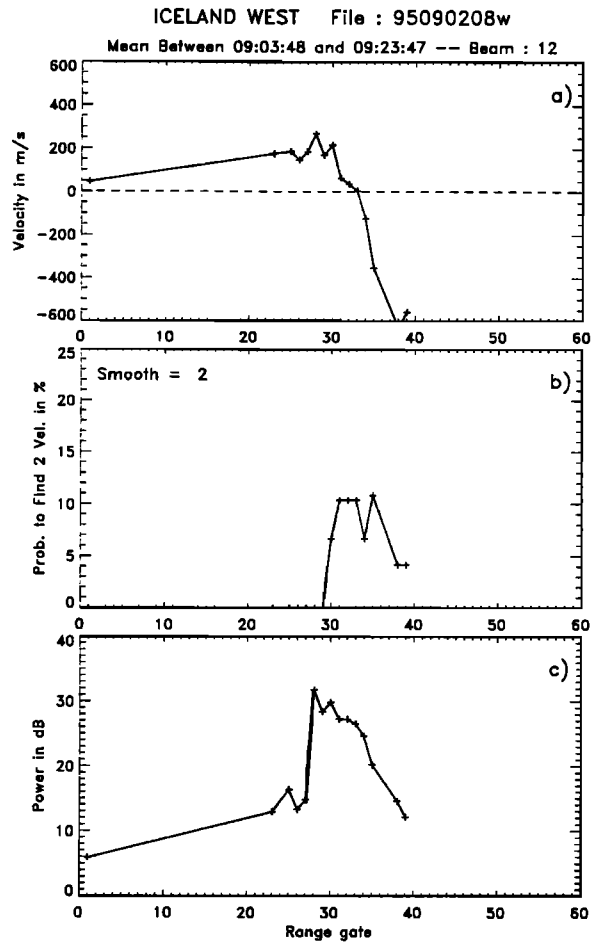



**Figure 9.** Analysis of a convection reversal with MUSIC. (a) Radial velocity. (b) Probability of multiple ionospheric sources. (c) Signal to noise ratio. The shear is characterized by an increased probability of multiple sources and an increased SNR.

MUSIC high-resolution spectral analysis technique can be used to handle more complex situations encountered where the signal includes several sources, due either to ground scatter or to multiple ionospheric lines. A statistical numerical simulation of SuperDARN data processed by the MUSIC method allows us to evaluate the performances and limits of applicability of the method. We also illustrate the capabilities of the MUSIC method with examples taken from experimental data.

We have shown that MUSIC is able to detect ionospheric sources superimposed on a ground echo. This capability depends strongly upon the spectral width; the larger the spectral width, the more difficult the separation. We have also shown that MUSIC is able to resolve multiple ionospheric sources, which are present in regions of inhomogeneous convection. The capability of MUSIC to separate several sources is a complex function of the SNR, the spectral width of the sources, and their separation. Low-velocity ionospheric echoes are particularly difficult to separate from ground scatter echoes.

Although no statistically significant evaluation has yet been done, it is clear that measurements with multiple sources are far from being the most common situation in SuperDARN data. This means that the much simpler and faster standard method of analysis, based on the single-source hypothesis, remains a very useful

and powerful tool. However, the results of the present study can be used to better define the limits of applicability of the standard method.

In further studies, the capability of MUSIC will be evaluated for other multipulse schemes giving a larger number of points in the ACF. The method will be also used for several geophysical purposes: (1) to reevaluate the physical interpretation of the spectral width in specific ionospheric regions; (2) to improve the accuracy of the localization of convection reversal boundaries; (3) to detect small-scale structures; and (4) to extend the field of ionospheric scatter to regions screened by ground scatter.

**Acknowledgements.** The Kapuskasing SuperDARN radar is operated by the Johns Hopkins University / Applied Physics Laboratory in the United States. The Stokkseyri SuperDARN radar is supported by Centre National de la Recherche Scientifique / Institut National des Sciences de l'Univers in France.

## References

Delhote, C., La haute résolution: Sa réalité et ses limites, *Trait. Signal, 2*, 112, 1985.

Farley, D. T., Multiple-pulse incoherent scatter correlation function measurements, *Radio Sci., 7*, 661, 1972.

Greenwald, R. A., K. B. Baker, R. A. Hutchins, and C. Hanuise, An HF phased-array radar for studying small-scale structures in the high-latitude ionosphere, *Radio Sci., 20*, 63, 1985.

Greenwald, R. A., et al., DARN/SuperDARN: A global view of the dynamics of high latitude convection, *Space Sci. Rev., 71*, 761, 1995.

Hanuise, C., J.-P. Villain, D. Grésillon, B. Cabrit, R. A. Greenwald, and K. B. Baker, Interpretation of HF radar ionospheric Doppler spectra by collective wave scattering theory, *Ann. Geophys., 11*, 29, 1993.

Marple, S. L., *Digital Spectral Analysis With Application, Signal Process. Ser.*, Prentice-Hall, Englewood Cliff, N.J.,1987.

Schmidt, R. O., Multiple emitter location and signal parameter estimation, *IEEE Trans. Antennas Propag., 34*, 276, 1986.

Villain, J.-P., R. A. Greenwald, K. B. Baker, and J. M. Ruohoniemi, HF radar observation of E region plasma irregularities produced by oblique electron streaming, *J. Geophys. Res., 92*, 12,327, 1987.

Villain, J.-P., R. André, C. Hanuise, and D. Grésillon, Observations of the high-latitude ionosphere by HF radars: Interpretation in terms of collective wave scattering and characterization of the turbulence. *J. Atmos. Sol. Terr. Phys., 58*, 943, 1996.

R. André, and J.-P. Villain, Laboratoire de Physique et Chimie de l'environnement, CNRS, 3A Avenue de la Recherche Scientifique, 45071 Orléans Cedex 2, France. (e-mail: raandre@cnrs-orleans.fr; jvillain@cnrs-orlean.fr)

L. Barthes, and J.-C. Cerisier, Centre d'Etude des Environnements Terrestre et Planétaires, UVSQ/CNRS, 4 Avenue de Nepture, 94107 Saint-Maur-des-Fossés Cedex, France. (e-mail: laurent.barthes@cetp.ipsl.fr; jean-claude.cerisier@cetp.ipsl.fr)

(Received October 24, 1997; revised February 24, 1998; accepted March 3, 1998.)